EBioMedicine 23 (2017) 25–33

Contents lists available at ScienceDirect

EBioMedicine

journal homepage: www.ebiomedicine.com

Research Paper

Dicyanomethylene Substituted Benzothiazole Squaraines: The Efficiency of Photodynamic Therapy *In Vitro* and *In Vivo*

Yongbiao Wei [a,e,1], Xiaoxiao Hu [c,1], Luyao Shen [a,b,1], Bing Jin [a], Xiangjun Liu [a,b], Weihong Tan [c,d,*], Dihua Shangguan [a,b,**]

[a] Beijing National Laboratory for Molecular Sciences, Key Laboratory of Analytical Chemistry for Living Biosystems, CAS Research/Education Center for Excellence in Molecular Sciences, Institute of Chemistry, Chinese Academy of Sciences, Beijing 100190, China
[b] University of the Chinese Academy of Sciences, Beijing 100049, China
[c] Molecular Science and Biomedicine Laboratory, State Key Laboratory of Chemo/Bio-Sensing and Chemometrics, College of Biology and College of Chemistry and Chemical Engineering, Hunan University Changsha, 410082, China
[d] Department of Chemistry, Center for Research at the Bio/Nano Interface, Health Cancer Center, UF Genetics Institute, McKnight Brain Institute, University of Florida Gainesville, FL 32611-7200, USA
[e] Department of Pharmaceutical Chemistry, School of Pharmaceutical Sciences, Guangxi Medical University, No. 22, Shuangyong Road, Nanning 530021, Guangxi, PR China

ARTICLE INFO

Article history:
Received 27 May 2017
Received in revised form 25 July 2017
Accepted 7 August 2017
Available online 9 August 2017

Keywords:
Photodynamic therapy
Near infrared photosensitizers
Squaraines
Cellular uptake

ABSTRACT

The lack of ideal photosensitizers limits the clinical application of photodynamic therapy (PDT). Here we report the PDT efficiency of dicyanomethylene substituted benzothiazole squaraine derivatives. This class of squaraine derivatives possess strong absorption and long excitation and emission wavelengths (ex/em, 685/720 nm). They show negligible dark toxicity, but can generate singlet oxygen under irradiation resulting in the apoptosis and necrosis of cells (phototoxicity). Changing the side chains of these compounds greatly influences their albumin-binding rate, cellular uptake and their phototoxicity. One of the squaraine derivatives with two methyl butyrate side chains shows high PDT efficiency in a mouse subcutaneous xenograft model under the irradiation of a 690 nm laser. These results show the great potential of dicyanomethylene substituted benzothiazole squaraines to be the leading compound of near-infrared photosensitizers in PDT.

1. Introduction

Photodynamic therapy (PDT), as a noninvasive and precisely directed method for cancer treatment, has attracted increasing attention recently. This therapy involves the combination of nontoxic photosensitizers and visible light. Under irradiation of light, photosensitizers in tumor cells produce a variety of reactive oxygen species (ROS). ROS attack the intracellular structures (*e.g.*, plasma membrane, mitochondria, lysosomes, and nuclei) by irreversible enzyme inactivation, lipid peroxidation, protein denaturation, and crosslinking, as well as other structural changes, which result in the damage of structure and function of cells (Bugaj, 2011; Lucky et al., 2015; Velema et al., 2014). In PDT, the photosensitizer plays a key role. The reported photosensitizers are mainly porphyrin-based derivatives (Lucky et al., 2015; Ormond and Freeman, 2013). Several classes of non-porphyrin derivatives, such as cyanines (Fekrazad et al., 2015; Gluth et al., 2015), xanthenes (Gianotti et al., 2014; Wang et al., 2013; Yao et al., 2014), phenothiazines (Samy et al., 2015; Yu et al., 2015), and anthraquinones (Sharma and Davids, 2012; Theodossiou et al., 2009) were investigated recently. Most of the reported photosensitizers absorb light in the visible region. An ideal photosensitizer should possess strong absorption in the wavelength range of 600–800 nm, where the tissue penetration by light is higher, with good yields of ROS and minimal dark toxicity (toxicity in the absence of light) (Avirah et al., 2012; Lucky et al., 2015; Ormond and Freeman, 2013). Additionally, good photosensitizers should possess favorable biodistribution, such as easily penetrating and retaining in target tissue. However, with these disparate requirements, few compounds can be qualified as an ideal photosensitizer.

Squaraines belong to a class of cyanine dyes composed of a central electron deficient four-membered ring core flanked by electron-rich aromatic moieties. They possess good light stability, sharp and intense absorption bands ($\varepsilon \sim 10^5\ M^{-1}\ cm^{-1}$) in the red to near-infrared (NIR) region, and high fluorescence quantum yield (Mayerhoffer et al., 2012, 2013; Song et al., 2009; Sreejith et al., 2008; Wang et al., 2010a,b). These photochemical and photophysical properties make squaraines

* Correspondence to: Weihong Tan, Molecular Science and Biomedicine Laboratory, State Key Laboratory of Chemo/Bio-Sensing and Chemometrics, College of Biology and College of Chemistry and Chemical Engineering, Hunan University Changsha, 410082, China.
** Correspondence to: Dihua Shangguan, Beijing National Laboratory for Molecular Sciences, Key Laboratory of Analytical Chemistry for Living Biosystems, CAS Research/Education Center for Excellence in Molecular Sciences, Institute of Chemistry, Chinese Academy of Sciences, Beijing 100190, China.
E-mail addresses: tan@chem.ufl.edu (W. Tan), sgdh@iccas.ac.cn (D. Shangguan).
[1] These authors contributed equally to this work.

http://dx.doi.org/10.1016/j.ebiom.2017.08.010

highly suitable for biological applications, such as fluorescent sensors, fluorescent labels (Jisha et al., 2010; Oswald et al., 1999; Patonay et al., 2004), and photosensitizers (Ramaiah et al., 1997, 2002, 2004; Santos et al., 2004). Although, some squaraines have been designed and synthesized as potential photosensitizers in PDT (Avirah et al., 2012), only a few reports describe the photosensitizing effects of these squaraines *in vivo* (Devi et al., 2008) or in cultured cells (Ramaiah et al., 2002, 2004).

Most recently, we synthesized a new dicyanomethylene substituted benzothiazole squaraine derivative (CSTS) (Scheme 1), which possesses a strong absorption band ($\varepsilon_{685\ nm} = 1.65 \times 10^5\ M^{-1}\ cm^{-1}$) and high fluorescence quantum yield (0.47). Because of the increased sterical congestion resulting from the dicyanomethylene substitution on the central four-membered ring, CSTS possesses a rigid π-conjugated planar structure (Jin et al., 2014). The dicyanomethylene substitution also results in a long ex/em wavelength of CSTS (ex/em, 685/720 nm). These properties make dicyanomethylene substituted benzothiazole squaraines potential near-infrared photosensitizers for PDT. However, CSTS cannot enter cell membranes, limiting its further application *in vivo*. In order to investigate the efficiency of dicyanomethylene substituted benzothiazole squaraines for PDT, in this paper we designed and synthesized three CSTS analogues (CSBE, CSME, and CSBM) (Scheme 1), and compared their photosensitizing effects in solution and in cultured cells. Additionally, we also tested the PDT efficiency of CSBE in a tumor xenograft mouse model.

2. Materials and Methods

2.1. Materials and Reagents

3,4-Diethoxycyclobut-3-ene-1,2-dione, malonodinitrile, 2-methyl-1,3-benzothiazole, and methyl 4-bromobutanoate were obtained from J&K Co., Ltd. HSA was purchased from Sigma and used without further purification. Cell counting Kit-8 (CCK-8) was purchased from Dojindo (Shanghai, China). Stock solutions of CSTS, CSBE, CSME, and CSBM (10 mM) were prepared in DMSO. All solutions were prepared with deionized water that was purified using a UPHW-III-90 T UP water purification system (Chengdu, China). All other ordinary solvents and chemical reagents were used as received without further purification.

2.2. Cell Lines

MCF-7 (breast cancer), PC-3 (prostate cancer) and A549 (non-small cell lung cancer) were bought from the Cell Resource Center of Shanghai Institute for Biological Sciences (Chinese Academy of Sciences, Shanghai); A549T (Taxol-resistant A549 subline) from Shanghai Aiyan Biological Technology Co., Ltd. (Shanghai, China); LoVo (colon cancer), HCT-8 (colon cancer) and K562 (chronic myelogenous leukemia) from Cell Culture Center of Institute of Basic Medical Sciences, Chinese Academy of Medical Sciences (Beijing, China). H1299 (non-small cell lung cancer) cells were purchased from ATCC (Manassas, VA). Cells were grown in DMEM (Hyclone) medium containing 10% fetal bovine serum (FBS, Gibco) in a humidified incubator with 5% CO_2 at 37 °C.

2.3. Instruments

^{1}H NMR spectra were collected with a Bruker Avance 400 MHz spectrometer using DMSO-d_6 as solvent. ESI-mass spectra (MS) were recorded with a LC-MS 2010A (Shimadzu) instrument. High-resolution MALD-TOF MS were collected with a Bruker Daltonics Flex-Analysis. Fluorescence spectra were measured on a Hitachi F-4500 fluorescence spectrofluorometer (Kyoto, Japan). UV–Vis spectra were collected with a UH5300 spectrophotometer (HITACHI, Japan).

2.4. Synthesis of CSBE, CSME, and CSBM

2.4.1. General Procedures

The synthesis route is illustrated in Scheme 2.

2.4.2. Triethylammonium 3-(Dicyanomethylene)-2-Ethoxy-4-Oxocyclobut-1-Enolate (1)

3,4-Diethoxycyclobut-3-ene-1,2-dione (340 mg, 2 mmol) was dissolved in anhydrous benzene (9 mL), and malonodinitrile (132 mg, 2 mmol) was added under stirring. Then triethylamine (0.26 mL) was added dropwise for 5 min. The obtained emulsion was stirred for 30 min at room temperature. The solvent was then removed using a rotary evaporator, and the crude product was purified on a silica gel column using ethyl acetate/methanol (10:1) as eluent, yielding 500 mg (86%) of desired product. ^{1}H NMR (400 MHz, MeOD) δ 4.73 (2H, q, J = 7.1 Hz), 3.24 (5H, q, J = 7.3Hz), 1.46 (3 H, t, J = 7.1 Hz), 1.33 (8H, t, J = 7.3 Hz).

2.4.3. General Procedure for the Synthesis of Compound 2

Compound 2 was prepared according to a previously reported method (Gromov et al., 1997). A mixture of 2-methyl benzothiazole (1.25 mL, 9.83 mmol), methyl γ-bromobutyrate (0.70 mL, 4.89 mmol), and iodomethane (0.70 mL) was heated for 6 h at 120 °C. After cooling to room temperature, the solution was added dropwise to an excess amount of diethylether to form a precipitate. The product was collected by filtration and then purified on a silica gel column using ethyl acetate/petroleum ether as eluent to afford the product.

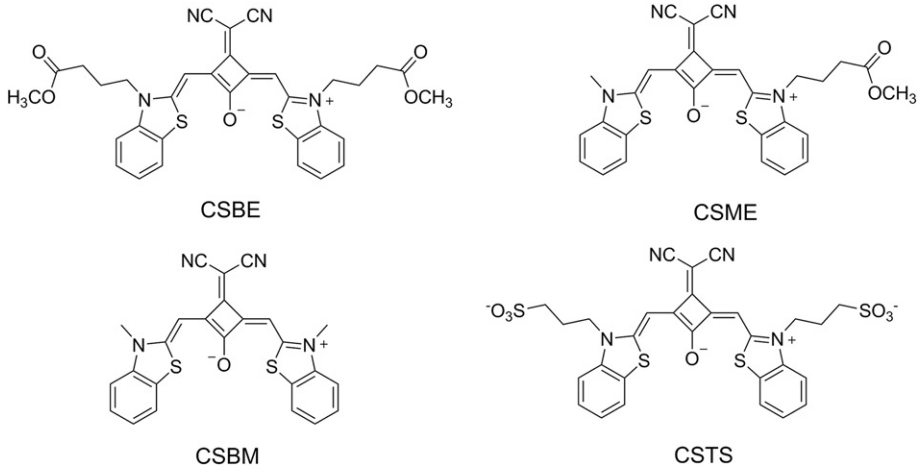

Scheme 1. Structures of CSBE, CSME, CSBM, and CSTS.

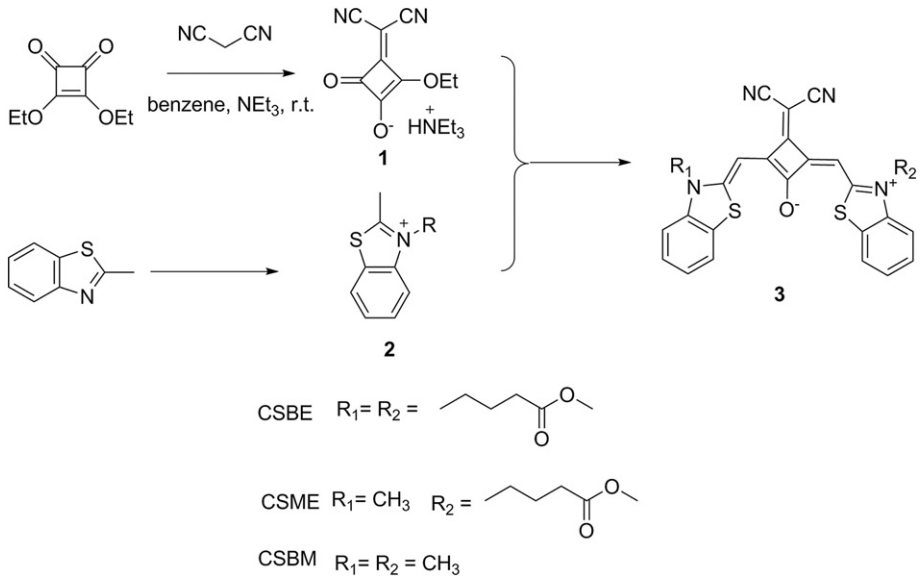

Scheme 2. Synthetic route of CSBE, CSME, and CSBM.

2.4.4. General Procedure for the Synthesis of CSBE, CSME, and CSBM

Functionalized squaric acid derivative 1 (291 mg, 1 mmol) and compound 2 (2 mmol) were heated to reflux in a 5:5:1 mixture of toluene, *n*-butanol, and quinolone (20 mL) using a Dean-Stark trap for 8 h. After cooling to room temperature, the solution was added dropwise to an excess amount of diethylether to form a precipitate. The residue was obtained after centrifugation and then purified on a silica gel column using DCM/methanol as eluent to afford the crude product. After a drying step under reduced pressure, the final compound was obtained.

2.4.5. (Z)-3-(Dicyanomethylene)-2-((Z)-(3-(4-Methoxy-4-Oxobutyl)Benzo[d]Thiazol-2(3H)-ylidene)Methyl)-4-((3-(4-Methoxy-4-Oxobutyl)Benzo[d]Thiazol-3-ium-2-yl)Methylene)Cyclobut-1-en-1-olate (CSBE)

^{1}H NMR (400 MHz, DMSO) δ 7.95 (2H, d, *J* = 7.7 Hz), 7.67 (2H, d, *J* = 8.1 Hz), 7.52 (2H, t, *J* = 7.4 Hz), 7.35 (2H, t, *J* = 7.4 Hz), 7.19 (1H, s), 6.64 (1H, s), 6.14 (2H, s), 5.32 (2H, s), 3.73 (6H, s), 2.00 (8H, m). HRMS (EI-TOF) calcd. for $C_{33}H_{28}N_4O_5S_2[M]^+$ 624.15011, found 624.14959.

2.4.6. (Z)-3-(Dicyanomethylene)-4-((3-(4-Methoxy-4-Oxobutyl)Benzo[d]Thiazol-3-ium-2-yl)Methylene)-2-((Z)-(3-Methylbenzo[d]Thiazol-2(3H)-ylidene)Methyl)Cyclobut-1-en-1-olate (CSME)

^{1}H NMR (400 MHz, DMSO) δ 7.96 (2H, d, *J* = 7.8 Hz), 7.67 (2H, d, *J* = 8.3 Hz), 7.55 (2H, t, *J* = 7.2Hz), 7.36 (2 H, t, *J* = 7.5 Hz), 7.21 (1H, s), 6.64 (1H, s), 6.14 (2H, s), 3.73 (6H, s), 2.04 (4H, m). HRMS (EI-TOF) calcd. for $C_{29}H_{22}N_4O_3S_2[M]^+$ 538.11333, found 538.11291.

2.4.7. (Z)-3-(Dicyanomethylene)-2-((Z)-(3-Methylbenzo[d]Thiazol-2(3H)-ylidene)Methyl)-4-((3-Methylbenzo[d]Thiazol-3-ium-2-yl)Methylene)Cyclobut-1-en-1-olate (CSBM)

^{1}H NMR (400 MHz, DMSO) δ 8.42 (2H, d, *J* = 8.4 Hz), 8.29 (2H, d, *J* = 8.5 Hz), 7.92 (2H, t, *J* = 7.8 Hz), 7.81 (2H, t, *J* = 7.7 Hz), 7.19 (1H, s), 6.65 (1H, s), 4.20 (6H, s). HRMS (EI-TOF) calcd. for $C_{25}H_{16}N_4OS_2[M]^+$ 452.07655, found 452.07582.

2.5. Interaction of CSTS, CSBE, CSME, and CSBM With Human Serum Albumin (HSA)

The interaction of compounds with HAS was investigated by UV–Vis absorption and fluorescence spectra. HSA stock solution was prepared by dissolving HSA directly into PBS (0.1 mM). Squaraines (4 μM) were mixed with different concentrations of HSA and kept in the dark overnight before the measurement for full association.

2.6. Measurement of Singlet Oxygen

The singlet oxygen ($^1O_2$) generation from the squaraines upon irradiation was studied using 1,3-diphenylisobenzofuran (DPBF) as the $^1O_2$ indicator(Yuan et al., 2015; Zimcik et al., 2009). DPBF reacts irreversibly with $^1O_2$ which causes a decrease in the intensity of the DPBF absorption band at 418 nm. In a typical experiment, an equal volume of DPBF in DMSO ($ABS_{418\ nm} = 1$) and squaraines in DMSO ($ABS_{690\ nm} = 0.5$) was mixed; the solutions were irradiated with a 690 nm laser at 6 mw/cm^2, and their absorbance at 418 nm was recorded with a UH5300 spectrophotometer after irradiation for 0, 5, 10, 15, 20, 25, 30, 35, and 40 s.

2.7. Confocal Imaging

Cells were seeded in a confocal dish (35 × 12 mm, Φ20 mm glass bottom) and grown for 24 h, then incubated with fresh medium (1 mL) containing squaraines (0.5 μM) and Lyso-Tracker Blue or Mito-Tracker Green for 1 h. After washed with PBS (pH 7.4) three times, cells were imaged under a confocal microscope (OLYMPUS FV1000-IX81, Olympus Corporation, Japan), using a 100× objective lens. The fluorescence of squaraines was excited at 635 nm and collected within 650–750 nm. The fluorescence of Lyso-Tracker Blue and Mito-Tracker Green were excited at 405 and 488 nm, respectively.

2.8. Photo-/Dark-Cytotoxicity

The dark cytotoxicity of these squaraines was tested with seven cancer cell lines (PC-3, MCF-7, HCT-8, A549, A549T, K562, and LoVo) using Cell Counting Kit-8 (CCK-8) kit (Dojindo Laboratories, Kumamoto, Japan). Briefly, cells (5 × 10^3/well) were seeded into 96-well plates and grown for 18 h; then added with compounds at different concentrations and further incubated for 48 h. Finally, the media were replaced with fresh media (100 μL) (without FBS) containing 10 μL of CCK-8 reagent and incubated for 1 h. The absorbance at 450 nm was collected on a plate reader (SpectraMax M5, Molecular Devices, CA, USA). The

cell survival percentage (SP) was calculated according to Eq. (1):

$$SP = \frac{A - A_0}{A_S - A_0} \times 100\% \quad (1)$$

where A, A_s and A_0 are the absorbance of experimental group, control group and blank group (no cells).

For photo-cytotoxicity, seven cancer cell lines (MCF-7, PC-3, H1299, A549, A549T, K562, and LoVo) was used. Briefly, cells (1×10^4 cells/well) grown in 96-well cell culture plates were incubated for 24 h with concentrations from 2 to 10 μM of compound. Then the plate was washed twice with warm PBS containing 2.5% FBS and incubated for 30 min. The cells were irradiated in a dark room with a 690 nm diode laser light at 150 mW/cm^2 to achieve a total light dose of 3.6 J/cm^2. Then the plates were further incubated at 37 °C for an additional 24 h, and the cell viability was measured with a CCK-8 kit as described above.

2.9. Cell Apoptosis Assay

The apoptosis assay of MCF-7 cells after treatment with CSBE was performed by flow cytometry assay with Annexin V-FITC Apoptosis Kit according to the vendor's instructions. This method is based on the detection of differences in phosphatidylserine on cytomembranes using Annexin V and the detection of membrane damage with propidium iodide (PI). Briefly, MCF-7 cells treated with CSBE (10 μM) for 24 h were irradiated with a total light dose of 3.6 J/cm^2 and were further cultured for 0, 1, 3, 6, 12, and 24 h. Then cells were double-stained with 200 μL of labeling solution containing FITC-labeled Annexin V and PI for 15 min at room temperature. Subsequently, the samples were analyzed with BD FACS Calibur with Cell Quest software (BD Bioscience, San Jose, CA) by counting 1×10^4 events with an excitation wavelength of 488 nm.

2.10. NIR Fluorescence Imaging In Vivo and Tissue Biodistribution

Athymic nude mice were obtained from Shanghai SLRC Laboratory Animal Co., Ltd. and maintained in a controlled environment and freely access to standard food and water. Prior to initiation of the experiments, mice were acclimatized to husbandry conditions for 1 week to eliminate the stress. All experiments were performed in strict compliance with the guide of the care and use of laboratory animals of Hunan University Laboratory Animal Center. The Hunan University Animal Study Committee approved the experiments. The xenografted tumors were established by subcutaneous injection of 5×10^6 H1299 cells into the right shoulder of female nude mice (4–5 week). Tumor size was measured daily using calipers, and allowed growing to 5–7 mm in diameter. The tumor-bearing nude mice were intraperitoneally, or intratumorally, injected (at the bottom of the tumor) with 50 μL of CSBE (3.25 mg/mL, 5 mM) or tail intravenously injected with 50 μL of CSBE (0.325 mg/mL, 0.5 mM). The mice were sacrificed at indicated time, and the major organs, including the tumor, liver, heart, lung, spleen, and kidney, were dissected and imaged with IVIS Lumina XR (Caliper Life Sciences) with an excitation band pass filter at 675/30 nm and an emission at 740/80 nm. A tumor-bearing mouse intratumorally injected with CSBE was anesthetized and imaged at pre-injection, 10 min, 1, 2, 6, 12, 24, 48, and 96 h post-injection with the imaging system as described above.

2.11. Photodynamic Treatment In Vivo

The H1299 cells xenografted tumors were established as described above. When the tumors had grown to an average size of 5–6 mm in diameter, the mice were randomly divided into four groups ($n = 6$) and administered through intratumoral injection (50 μL at the bottom of the tumor) with a) PBS, b) PBS + light, c) CSBE (3.25 mg/mL, 5 mM in PBS), and d) CSBE + light. Tumors in mice of group b and d were irradiated with a NIR laser (690 nm, 500 mW/cm^2) for 15 min after 24 h post-injection. Two days later, therapeutic agents were injected again, and mice were again subjected to NIR light irradiation for 15 min after further injection 24 h as mentioned above. The body weight of mice and tumor size were measured daily. The tumor volume was calculated according to the formula of V = 1/2 (larger diameter) × (smaller diameter)^2. When the tumor size in control groups reached ~1600 mm^3, tumors and major organs were collected from tumor-bearing mice and embedded in OCT (an embedding medium used for frozen tissue) and frozen at − 80 °C. Histological examination was performed using Pannoramic MIDI (3DHistech Ltd., Budapest, Hungary) after stained the tissue sections with hematoxylin and eosin (H&E).

2.12. Statistical Analysis

All data are presented as mean ± SD. The statistical analysis was performed by One-way analysis of variance (ANOVA). Statistical significance was accepted at the level of $p < 0.05$.

3. Results

3.1. Design and Synthesis of CSBE, CSME, and CSBM

Previously, we synthesized a new squaraine derivative, CSTS, which possesses a crescent-shaped π-conjugated planar core (Jin et al., 2014). The photophysical properties of CSTS suggest that it holds great promise as a photosensitizer in PDT. However, our recent study indicated that CSTS cannot enter cells, which limits its further application in PDT. CSTS carries two sulfonic groups, which may hinder its penetration into the negatively charged cell membrane. Because the photophysical properties of CSTS are mainly contributed by the dicyanomethylene substituted benzothiazole squaraine core, it is possible to obtain new dicyanomethylene substituted squaraines for PDT investigation by changing the side chains of CSTS. In order to improve the cellular uptake, three CSTS analogues (CSBE, CSME, and CSBM) were designed and synthesized by displacing negatively charged sulfonic acid groups with electrically neutral methyl or methyl butanoate groups. The PDT effects of these compounds were investigated.

3.2. Absorption and Emission Spectra of CSBE, CSME, and CSBM

Cyanine dyes usually self-aggregate in aqueous solution *via* van der Waals forces and π–π stacking interactions. CSTS was reported to mainly form H-aggregates in aqueous solution (Jin et al., 2014). Thus the absorption and emission spectra of CSBE, CSME, and CSBM were measured in mixed solutions of water and DMSO (Fig. 1). These three compounds showed a very broad and low absorption band around 600 nm in water, suggesting their aggregation. With increasing DMSO content (V_{DMSO}/V_{H2O}: 0/10–10/0), the absorption band of these compounds increased, red-shifted and finally became a sharp band around 670–690 nm when the DMSO content reached 60% (CSBE), 70% (CSME), or 80% (CSBM) (see Fig. 1a), suggesting the transformation from H-aggregate form to monomer form of these compounds. The emission spectra showed almost no fluorescence emission of these compounds at low DMSO content, and then an increasing fluorescence band (710–745 nm) with increasing DMSO content (see Fig. 1b), which corresponded well to the increase of the absorption band around 670–690 nm. These results indicate that these compounds have the same absorption and fluorescence spectra as that of CSTS. Based on the content of DMSO that caused the change of absorption and emission, the aggregation tendency of these compound was CSBE < CSME < CSBM.

3.3. Binding of CSTS, CSBE, CSME, and CSBM to HSA

The binding to plasma proteins can significantly influence the therapeutic, pharmacodynamic, and toxicological action of drugs, such as

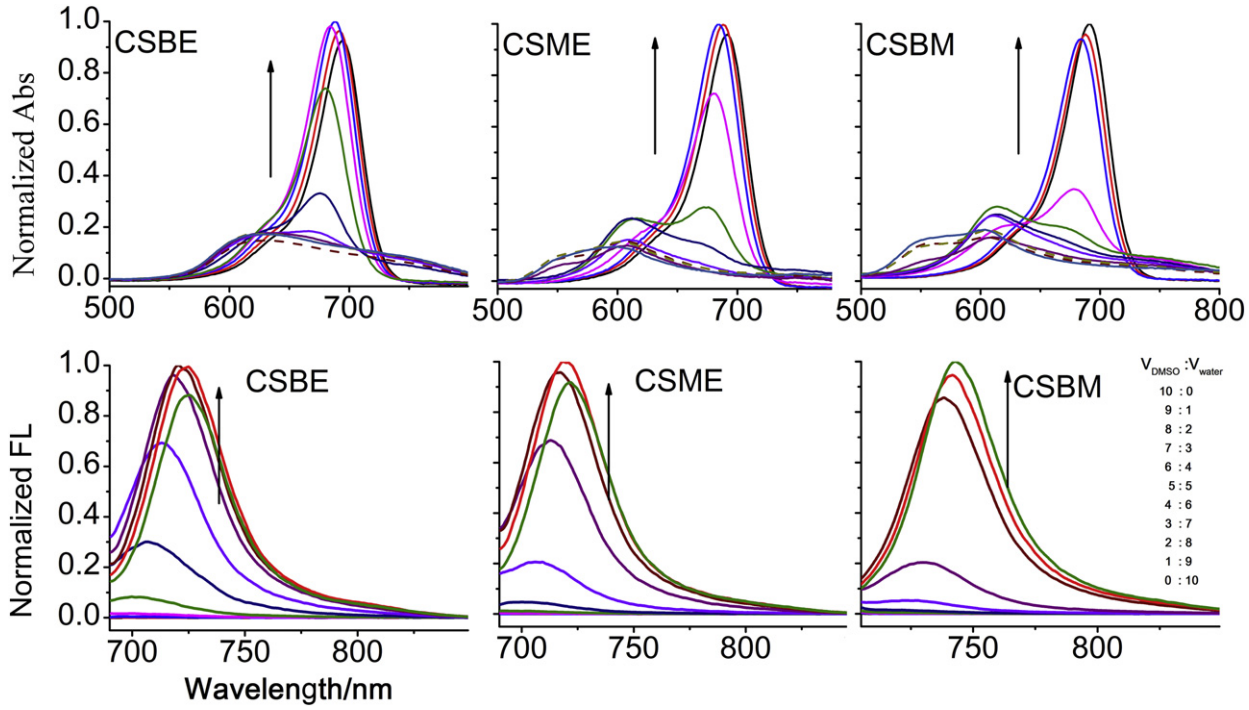

Fig. 1. Absorption (a) and fluorescence spectra (b) of CSBE, CSME, and CSBM (10 μM) in mixed solutions of DMSO and water, with excitation at 670 nm.

absorption, distribution, cellular uptake, and clearance properties. It is generally accepted that only the free drug in plasma is available to elicit a pharmacological effect. Because human serum albumin (HSA) is the most abundant protein in human blood plasma, the interaction of CSBE, CSME, CSBM, and CSTS with HSA was investigated. Fig. 2 shows the absorption and emission spectra of these compounds in the presence of different concentrations of HSA. In the absence of HSA, the absorption spectra of CSTS in PBS show a broad band with a peak at around 600 nm and a shoulder around 690 nm, and CSBE, CSME, and CSBM show a very broad band with the maximum around 600 nm (broken line), suggesting the heavier aggregation of these compounds than that of CSTS. The addition of HSA to these compounds only caused a remarkably spectral change of CSTS (Fig. 2), that is, the absorption peak red-shifted to around 690 nm and increased with the rise of HSA concentration; the addition of HSA did not affect the absorption spectra of CSBE, CSME, and CSBM. Furthermore, the addition of HSA did not change the fluorescence spectra of CSBE, CSME, and CSBM, but greatly enhanced the fluorescence of CSTS. These results suggest that only CSTS bound to HSA and was located in a hydrophobic environment, which may due to its negatively charged sulfonate groups. The negligible HSA binding of CSBE, CSME, and CSBM implies the potential to act as photosensitizers in PDT.

3.4. Singlet Oxygen Measurements

The $^1O_2$ generation upon the irradiation of a photosensitizer with light plays a key role in photodynamic therapy. The $^1O_2$ generation from these four squaraines upon irradiation was measured by using 1,3-diphenylisobenzofuran (DPBF) as the $^1O_2$ indicators (Yuan et al., 2015). In the absence of these compounds, the absorbance of DPBF at 418 nm decreased slightly by <10% after irradiation under a 690 nm laser beam for 40 s. However, in the presence of these four compounds, the DPBF absorbance decreased with increased irradiation time and decreased by 65% (CSTS) and 75% (CSBE, CSME, and CSBM) after

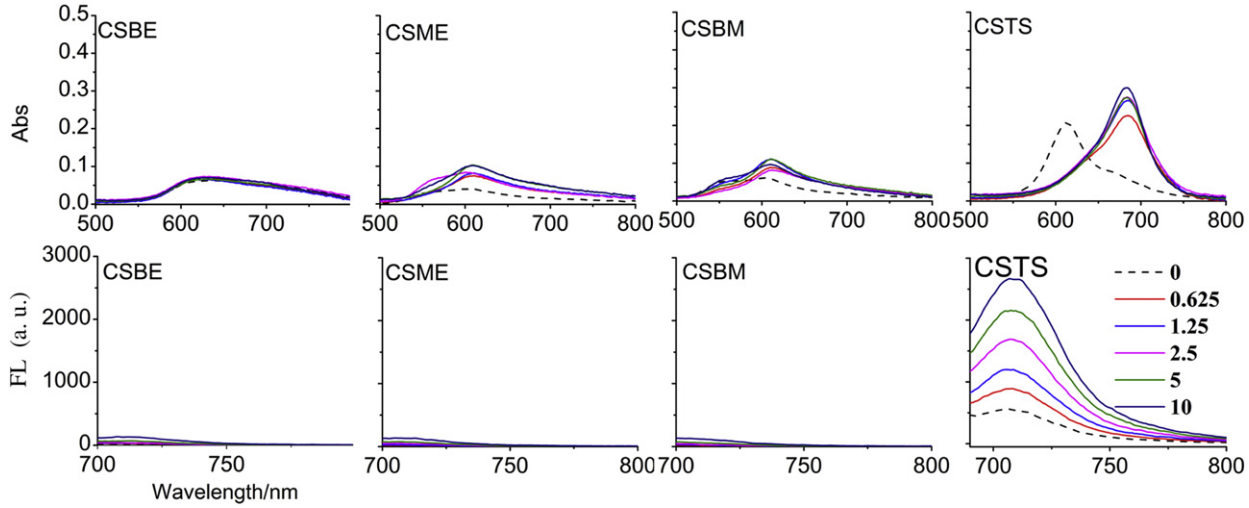

Fig. 2. Absorption (a) and fluorescence spectra (b) of CSBE, CSME, CSBM, and CSTS (4 μM) with different concentrations of HSA (0, 0.625, 1.25, 2.5, 5, and 10 μM).

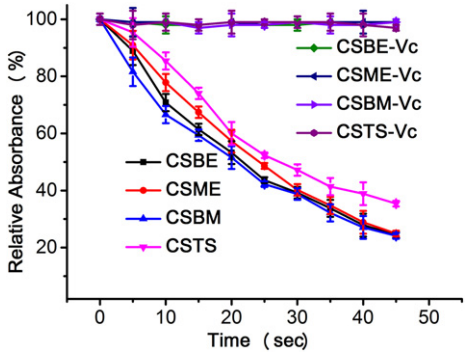

Fig. 3. Plots of the relative absorbance change of DPBF *versus* irradiation time in CSBE, CSME, CSBM, and CSTS solutions with and without vitamin C (VC). The data shown are mean values ± standard deviation, $n = 3$.

irradiation for 40 s (Fig. 3). Furthermore, the addition of $^1O_2$ scavenger, vitamin C, almost totally inhibited the decrease of the absorbance of DPBF. These results suggest that these compounds can generate $^1O_2$ under the irradiation at 690 nm.

3.5. Cellular Uptake and Intracellular Localization of CSBE, CSME, CSBM, and CSTS

The cellular uptake and subcellular localization of photosensitizers play a key role in PDT (Noodt et al., 1999). In order to evaluate the feasibility of these compounds as photosensitizers, we compared the cellular uptake and localization of these compounds. Confocal imaging showed that CSTS could not enter living cells, while the other three compounds were able to enter living cells. CSBE and CSME with one and two methyl butanoate side chains, respectively, exhibited higher cellular uptake than CSBM based on the fluorescence intensity in cells. The co-staining with Mito-Tracker Green (mitochondria probe) and Lyso-Tracker Blue (lysosome probe) showed that these three dyes were mainly located in lysosomes (Fig. 4). Flow cytometry assay further showed that the order of cellular uptake of these compounds was CSBE > CSME > CSBM > CSTS (Fig. S1). The low uptake of CSTS may be due to its negatively charged sulfonate groups that do not facilitate penetration through cell membranes. These results suggest that the side arms on squaraines greatly influence their cellular uptake.

3.6. Dark- and Photo-Cytotoxicity

The dark- and photo-cytotoxicity of these compounds were assessed by Cell Counting Kit-8 (CCK-8) assay. For dark-cytotoxicity assay, MCF-7, A549, A549T, PC-3, HCT-8, K562, and Lovo cells were incubated with different concentrations (2 to 100 μM) of these compounds for 48 h without irradiation. The survival of all these cells was >95% even where the concentration of these compounds was as high as 100 μM (Fig. 5b), suggesting the low cytotoxicity of these compounds. The photo-cytotoxicity assay was firstly tested on MCF-7 cells. MCF-7 cells were incubated with different concentrations of these compounds for 24 h, and then irradiated under a 690 nm laser beam to achieve a total light dose of 3.6 J/cm^2; the cell viability was measured after further incubation for 24 h. As shown in Fig. 5a, CSTS did not show significant photo-cytotoxicity, while CSBE, CSME, and CSBM showed dose-dependent photo-cytotoxicity. CSBE showed the strongest photo-cytotoxicity with IC_{50} values of 1.135 μM. The order of the photo-cytotoxicities of these compounds was CSBE > CSME > CSBM > CSTS, which is consistent with their cellular uptake. Further photo-cytotoxicity assay of CSBE and CSME on other six cell lines showed similar results as on MCF-7 (Fig. S2). The negligible dark-cytotoxicity but remarkable photo-cytotoxicity of CSBE, as well as its activation by long wavelength laser beam, makes it hold significant photochemotherapeutic potential.

3.7. Cell Apoptosis and Necrosis Induced by CSBE After Irradiation

To further investigate the possible photo-cytotoxicity mechanism of the dicyanomethylene substituted benzothiazole squaraines, the Annexin V-fluorescein/PI assay was performed to explore the apoptotic profiles of MCF-7 cells after treatment with CSBE and irradiation. As shown by Fig. 6, most cells were alive after the irradiation treatment (the result of 0 h). However, after further culture of the treated cells, the number of early apoptotic cells (lower right quadrants (Annexin V^+ and PI^-)) and late apoptotic/dead cells (upper right quadrants (Annexin V^+ and PI^+)) increased with culture time. After culturing for 24 h, 70% of cells were in apoptotic stage or dead. This set of results suggests that treatment with CSBE and irradiation did not directly cause the

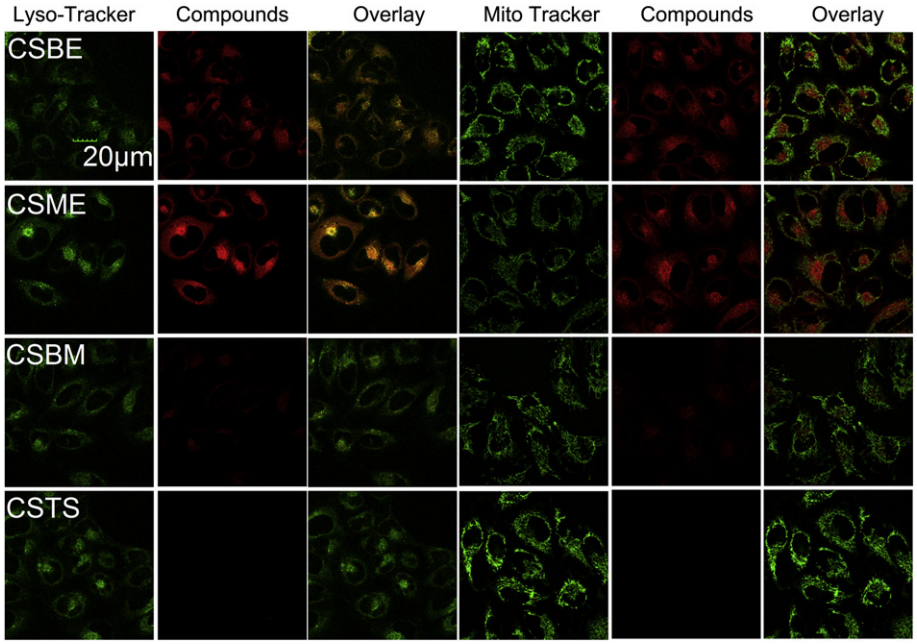

Fig. 4. Confocal images of MCF-7 cells stained by CSBE, CSME, CSBM or CSTS (0.5 μM) (λex = 635 nm), Mito-Tracker Green (λex = 488 nm), and Lyso-Tracker Blue (λex = 405 nm).

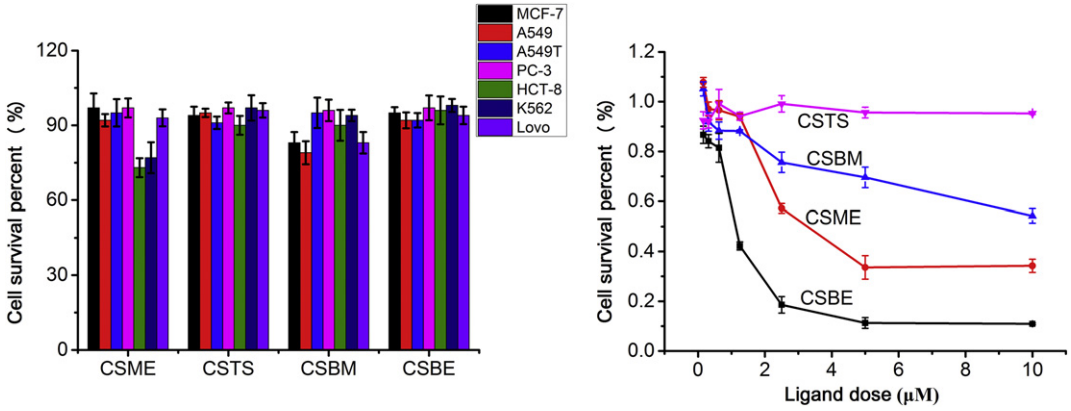

Fig. 5. Dark- and photo-cytotoxicity (a) Viability of different cells after treatment with CSBE, CSME, CSBM, and CSTS (100 μM) in the dark. (b)Viability of MCF-7 cells treated with variable concentrations of CSBE, CSME, CSBM, and CSTS and irradiated under a 690 nm laser beam.

cell damage immediately; the attack by $^1O_2$ generated by photo-activated CSBE caused the apoptosis and the necrosis of cells.

3.8. *In Vivo* Study

The excellent photodynamic effect *in vitro* of CSBE motivated us to investigate the photodynamic therapy *in vivo*. To reveal the distribution *in vivo*, we intraperitoneally, tail intravenously, or intratumorally injected mice with CSBE and examined the *ex vivo* fluorescence distribution in organs. After tail intravenous or intraperitoneal injection, the fluorescence of CSBE was observed in tumor, liver, kidney, lung, and spleen tissues but not in heart tissues (Fig. S3a). After intratumoral injection, the fluorescence of CSBE was also found in tumor, liver, kidney, lung, and spleen tissues, suggesting that CSBE can not only target tumors but also other organs *in vivo*. By intratumoral injection (at the bottom of the tumor), the strong fluorescence in tumor was observed at ten minutes; then the fluorescence reached the maximum at 1 h and lasted to 6 h, and then gradually reduced until 72 h (Fig. S3b).

To ensure the same amount of CSBE in tumors, we used intratumoral injection for further photodynamic therapy. When the tumors grew to a size of 5–6 mm in diameter, 24 mice were divided into four groups randomly (6 mice/group) and then treated with: a) PBS, b) PBS + light, c) CSBE, and d) CSBE + light respectively. The mice from control groups (a) and (c) were not irradiated, while the mice from control group (b) and experimental group (d) were exposed to a 690 nm laser (500 mW/cm^2) as described in section 2.11 (Fig. 7a). The body weights were recorded, and the tumor sizes were measured daily after the above treatments. The mean body weights of all the groups did not change much (~20 g) (Fig. S4) within 14 days. In the PBS, PBS + light, and CSBE groups, the tumor sizes of all mice were significantly increased, and reached ~1.6 cm^3 within 14 days after treatment (Fig. S5). The tumor volumes of all mice in these groups changed as a function of time (Fig. 7b and c), and showed indistinguishable growth rates among these groups, suggesting that only laser irradiation or CSBE injection did not affect the tumor development. However, in all 6 mice in the CSBE + light group, tumor sizes were gradually reduced compared with that in the PBS group ($p < 0.05$). These results suggest the innocuity and the excellent photodynamic effect of CSBE *in vivo*.

In addition, the histological examination of the tumors, liver, and kidney slices was performed after treatment for 14 days. Compared with the tumor sections from the three control groups, cell damage were observed in the tumors with both CSBE injection and laser

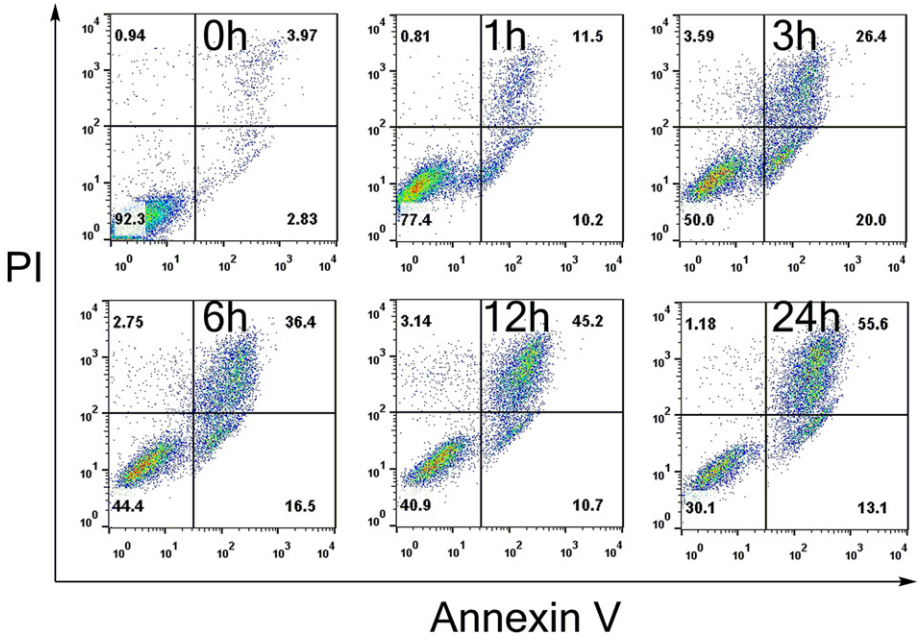

Fig. 6. Apoptosis and necrosis of MCF-7 cells after treatment with CSBE and irradiation. Viable cells are Annexin V$^-$/PI$^-$. The Annexin V$^+$/PI$^-$ cells are early in the apoptosis process, whereas the Annexin V$^+$/PI$^+$ represent late-apoptotic or necrotic cells.

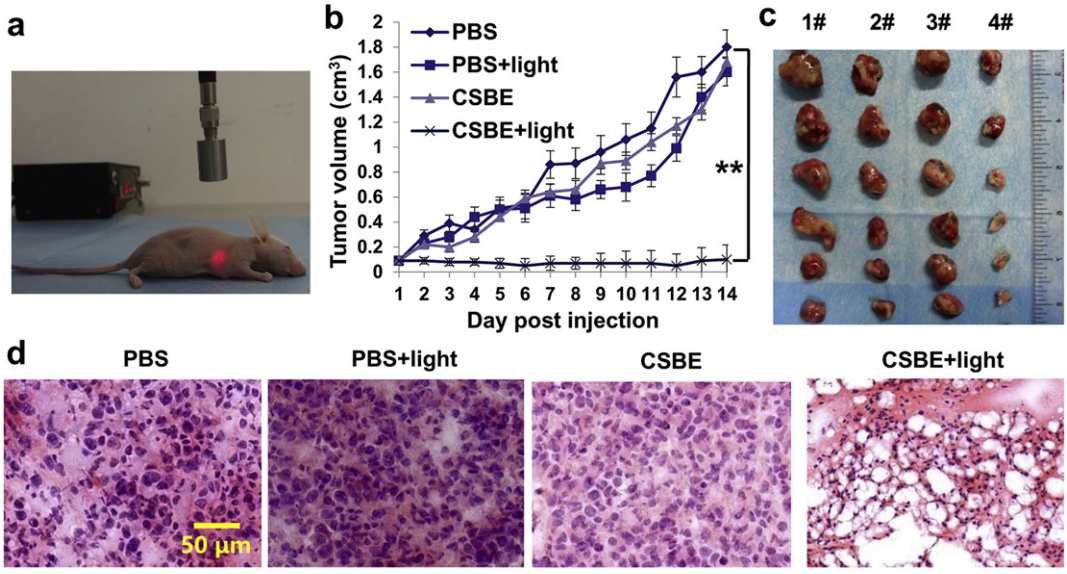

Fig. 7. Photodynamic therapy results of CSBE. a) Photodynamic therapy set-up showing laser light and a tumor-bearing mouse. b) Average tumor volumes of each group of mice bearing H1299 tumors. Each point represents the mean SD ($n = 6$ for each group). c) Tumor images for each group ($n = 6$). Column 1#–4#: PBS, PBS + light, CSBE, CSBE + light. d) Pathological features of tumors in representative mice in each group where the tumor slices of mice were stained with hematoxylin and eosin.

irradiation (Fig. 7d). The treatment in the CSBE + light group results in severe cellular damage, such as cell lysis, shrinkage, and nuclear condensation. Thus, the PDT of cancer combined with CSBE injection and 690 nm laser irradiation is a highly effective and feasible. It is worthwhile to note that the histological examination of liver and kidney slices did not found any cell injury (Fig. S6), further confirming the innocuity of CSBE.

4. Discussion

On the basis of the results of the *in vitro* study, we confirmed the innocuity and high PDT efficacy of CSBE using a nude mouse xenograft *in vivo* model. One limitation of CSBE is the lack of tumor targeting. However, the *in vitro* results showed that the high PDT efficiency of CSBE was mainly determined by its dicyanomethylene substituted benzothiazole squaraine core structure. The side chains on this squaraine core structure mainly affected the pharmacokinetic properties of its derivatives. Therefore, through modification with different side chains and immobilization with targeting units (*e.g.* folic acid, gefitinib, gleevec, RGD peptide, antibody and even nanoparticles) on this dicyanomethylene substituted benzothiazole squaraine core, it is possible to obtain ideal photosensitizers for PDT.

In summary, three CSTS analogues (CSBE, CSME, and CSBM) with electrically neutral side chains were synthesized. Compared with CSTS, these synthesized compounds exhibited similar optical properties and singlet oxygen yield under irradiation, and exhibited much lower HSA binding rates. All these compounds showed very low dark-cytotoxicity, but exhibited different photo-cytotoxicities with the order of CSBE > CSME > CSBM > CSTS, which is consistent with the cellular uptake efficiency of these compounds. *In vivo* experiments demonstrated that under irradiation of a 690 nm laser, CSBE could totally inhibit the tumor growth by damaging cells, suggesting the high efficacy as a photosensitizer in PDT.

Funding Sources

This work was supported by Grant 973 Program (2013CB933700), NSF of China (21575147, 21375135, 21535009, 21635008 and 21621062) and 2016GXNSFAA380208.

Conflicts of Interest

The authors declare no conflicts of interest.

Author Contributions

D.S., Y.W., X.H. and L.S. conceived and designed the study. Y.W. synthesized the compounds and performed the spectral experiments. Y. W. and L.S. performed the cell experiments. X.H. and L.S. performed the animal experiments. Y. W., X.H., B.J., L.S., D.S. and X.L. analyzed the data. Y.W., X.H., D.S. and W.T. wrote the manuscript. D.S. and W.T. directed the overall project.

Appendix A. Supplementary Data

Supplementary data to this article can be found online at http://dx.doi.org/10.1016/j.ebiom.2017.08.010.

References

Avirah, R.R., Jayaram, D.T., Adarsh, N., Ramaiah, D., 2012. Squaraine dyes in PDT: from basic design to in vivo demonstration. Org. Biomol. Chem. 10 (5), 911–920.
Bugaj, A.M., 2011. Targeted photodynamic therapy - a promising strategy of tumor treatment. Photochem. Photobiol. Sci. 10 (7), 1097–1109.
Devi, D.G., Cibin, T.R., Ramaiah, D., Abraham, A., 2008. Bis(3,5-diiodo-2,4,6-trihydroxyphenyl)squaraine: a novel candidate in photodynamic therapy for skin cancer models in vivo. J. Photochem. Photobiol. B 92 (3), 153–159.
Fekrazad, R., Barghi, V.G., Mir, A.P.B., Shams-Ghahfarokhi, M., 2015. In vitro photodynamic inactivation of *Candida albicans* by phenothiazine dye (new methylene blue) and Indocyanine green (EmunDo (R)). Photodiagn. Photodyn. Ther. 12 (1), 52–57.
Gianotti, E., Estevao, B.M., Cucinotta, F., Hioka, N., Rizzi, M., Reno, F., et al., 2014. An efficient rose bengal based nanoplatform for photodynamic therapy. Chem. Eur. J. 20 (35), 10921–10925.
Gluth, M.B., Kaufmann, Y.C., Dornhoffer, J.L., Ferguson, S., 2015. Immunotargeted photodynamic therapy for cholesteatoma: in vitro results with anti-EGFR-coated indocyanine green nanocapsules. Otol. Neurotol. 36 (1), 76–81.
Gromov, S.P., Fedorova, O.A., Vedernikov, A.I., Fedorov, Y.V., Alfimov, M.V., 1997. Crown ether styryl dyes .21. Synthesis, spectral properties, and complex formation of trans isomers of the chromogenic dithia-15(18)-crown-5(6) ethers. Russ. Chem. B 46 (5), 967–974.
Jin, B., Zhang, X., Zheng, W., Liu, X.J., Zhou, J., Zhang, N., et al., 2014. Dicyanomethylene-functionalized squaraine as a highly selective probe for parallel G-quadruplexes. Anal. Chem. 86 (14), 7063–7070.
Jisha, V.S., Arun, K.T., Hariharan, M., Ramaiah, D., 2010. Site-selective interactions: squaraine dye-serum albumin complexes with enhanced fluorescence and triplet yields. J. Phys. Chem. B 114 (17), 5912–5919.

Lucky, S.S., Soo, K.C., Zhang, Y., 2015. Nanoparticles in photodynamic therapy. Chem. Rev. 115 (4), 1990–2042.
Mayerhoffer, U., Fimmel, B., Wurthner, F., 2012. Bright near-infrared fluorophores based on squaraines by unexpected halogen effects. Angew. Chem. Int. Ed. 51 (1), 164–167.
Mayerhoffer, U., Gsanger, M., Stolte, M., Fimmel, B., Wurthner, F., 2013. Synthesis and molecular properties of acceptor-substituted squaraine dyes. Chem. Eur. J. 19 (1), 218–232.
Noodt, B.B., Berg, K., Stokke, T., Peng, Q., Nesland, J.M., 1999. Different apoptotic pathways are induced from various intracellular sites by tetraphenylporphyrins and light. Br. J. Cancer 79 (1), 72–81.
Ormond, A.B., Freeman, H.S., 2013. Dye sensitizers for photodynamic therapy. Materials 6 (3), 817–840.
Oswald, B., Patsenker, L., Duschl, J., Szmacinski, H., Wolfbeis, O.S., Terpetschnig, E., 1999. Synthesis, spectral properties, and detection limits of reactive squaraine dyes, a new class of diode laser compatible fluorescent protein labels. Bioconjug. Chem. 10 (6), 925–931.
Patonay, G., Salon, J., Sowell, J., Strekowski, L., 2004. Noncovalent labeling of biomolecules with red and near-infrared dyes. Molecules 9 (3), 40–49.
Ramaiah, D., Joy, A., Chandrasekhar, N., Eldho, N.V., Das, S., George, M.V., 1997. Halogenated squaraine dyes as potential photochemotherapeutic agents. Synthesis and study of photophysical properties and quantum efficiencies of singlet oxygen generation. Photochem. Photobiol. 65 (5), 783–790.
Ramaiah, D., Eckert, I., Arun, K.T., Weidenfeller, L., Epe, B., 2002. Squaraine dyes for photodynamic therapy: study of their cytotoxicity and genotoxicity in bacteria and mammalian cells. Photochem. Photobiol. 76 (6), 672–677.
Ramaiah, D., Eckert, I., Arun, K.T., Weidenfeller, L., Epe, B., 2004. Squaraine dyes for photodynamic therapy: mechanism of cytotoxicity and DNA damage induced by halogenated squaraine dyes plus light (>600 nm). Photochem. Photobiol. 79 (1), 99–104.
Samy, N.A., Salah, M.M., Ali, M.F., Sadek, A.M., 2015. Effect of methylene blue-mediated photodynamic therapy for treatment of basal cell carcinoma. Lasers Med. Sci. 30 (1), 109–115.
Santos, P.F., Reis, L.V., Almeida, P., Serrano, J.P., Oliveira, A.S., Ferreira, L.F.V., 2004. Efficiency of singlet oxygen generation of aminosquarylium cyanines. J. Photoch. Photobio. A 163 (1–2), 267–269.
Sharma, K.V., Davids, L.M., 2012. Hypericin-PDT-induced rapid necrotic death in human squamous cell carcinoma cultures after multiple treatment. Cell Biol. Int. 36 (12), 1261–1266.
Song, B., Zhang, Q., Ma, W.H., Peng, X.J., Fu, X.M., Wang, B.S., 2009. The synthesis and photostability of novel squarylium indocyanine dyes. Dyes Pigments 82 (3), 396–400.
Sreejith, S., Carol, P., Chithra, P., Ajayaghosh, A., 2008. Squaraine dyes: a mine of molecular materials. J. Mater. Chem. 18 (3), 264–274.
Theodossiou, T.A., Hothersall, J.S., De Witte, P.A., Pantos, A., Agostinis, P., 2009. The multifaceted photocytotoxic profile of hypericin. Mol. Pharm. 6 (6), 1775–1789.
Velema, W.A., Szymanski, W., Feringa, B.L., 2014. Photopharmacology: beyond proof of principle. J. Am. Chem. Soc. 136 (6), 2178–2191.
Wang, B.S., Fan, J.L., Sun, S.G., Wang, L., Song, B., Peng, X.J., 2010a. 1-(Carbamoylmethyl)-3H-indolium squaraine dyes: synthesis, spectra, photo-stability and association with BSA. Dyes Pigments 85 (1–2), 43–50.
Wang, W.H., Fu, A., Lan, J.B., Gao, G., You, J.S., Chen, L.J., 2010b. Rational design of fluorescent bioimaging probes by controlling the aggregation behavior of squaraines: a special effect of ionic liquid pendants. Chem. Eur. J. 16 (17), 5129–5137.
Wang, J.H., Wang, B.K., Liu, Q., Li, Q., Huang, H., Song, L., et al., 2013. Bimodal optical diagnostics of oral cancer based on rose bengal conjugated gold nanorod platform. Biomaterials 34 (17), 4274–4283.
Yao, M., Gu, C., Doyle, F.J., Zhu, H., Redmond, R.W., Kochevar, I.E., 2014. Why is rose bengal more phototoxic to fibroblasts in vitro than in vivo? Photochem. Photobiol. 90 (2), 297–305.
Yu, J.S., Hsu, C.H., Huang, C.C., Chang, P.Y., 2015. Development of therapeutic au-methylene blue nanoparticles for targeted photodynamic therapy of cervical cancer cells. ACS Appl. Mater. Interfaces 7 (1), 432–441.
Yuan, Y.Y., Zhang, C.J., Gao, M., Zhang, R.Y., Tang, B.Z., Liu, B., 2015. Specific light-up bioprobe with aggregation-induced emission and activatable photoactivity for the targeted and image-guided photodynamic ablation of cancer cells. Angew. Chem. Int. Ed. 54 (6), 1780–1786.
Zimcik, P., Miletin, M., Novakova, V., Kopecky, K., Dvorakova, Z., 2009. Tetrapyrazinoporphyrazines with different number of peripheral pyridyl rings: synthesis, photophysical and photochemical properties. Dyes Pigments 81 (1), 35–39.